This article has been amended to include a factual correction. An error was identified subsequent to its original publication. This error was acknowledged on page 360, volume 37, issue 05. The online article and its erratum are considered the version of record.

🔓 Open Access

Interferometric Ex Vivo Evaluation of the Spatial Changes to Corneal Biomechanics Introduced by Topographic CXL: A Pilot Study

Abby Wilson, MEng, PhD; John Jones, BEng; John Marshall, PhD, FRCPath

ABSTRACT

PURPOSE: To determine the efficacy of interferometry for examining the spatial changes to the corneal biomechanical response to simulated intraocular pressure (IOP) fluctuations that occur after corneal cross-linking (CXL) applied in different topographic locations.

METHODS: Displacement speckle pattern interferometry (DSPI) was used to measure the total anterior surface displacement of human and porcine corneas in response to pressure variations up to 1 mm Hg from a baseline pressure of 16.5 mm Hg, both before and after CXL treatment, which was applied in isolated topographic locations (10-minute riboflavin soak [VibeX-Xtra; Avedro, Inc], 8-minute ultraviolet-A exposure at 15 mW/cm²). Alterations to biomechanics were evaluated by directly comparing the responses before and after treatment for each cornea.

RESULTS: Before CXL, the corneal response to loading indicated spatial variability in mechanical properties. CXL treatments had a variable effect on the corneal response to loading dependent on the location of treatment, with reductions in regional displacement of up to 80% in response to a given pressure increase.

CONCLUSIONS: Selectively cross-linking in different topographic locations introduces position-specific changes to mechanical properties that could potentially be used to alter the refractive power of the cornea. Changes to the biomechanics of the cornea after CXL are complex and appear to vary significantly depending on treatment location and initial biomechanics. Hence, further investigations are required on a larger number of corneas to allow the development of customized treatment protocols. In this study, laser interferometry was demonstrated to be an effective and valuable tool to achieve this.

[*J Refract Surg.* 2021;37(4):263-273.]

Corneal cross-linking (CXL) via riboflavin and ultraviolet-A exposure has been shown to increase the stiffness of the cornea[1,2] and its resistance to deformation under intraocular pressure (IOP) via initiating the formation of covalent cross-links between different molecules in the corneal stroma.[3] Recently, CXL treatment has been shown to be effective for halting the progression, and in some cases causing beneficial refractive modifications, in keratoconic and ectatic corneas.[4-7]

Changes to the topography of the corneas that have been achieved, in some cases[8,9] when using CXL for the treatment of keratoconus have led to interest in the potential of CXL to be employed for refractive correction via selectively stiffening different regions of the cornea in isolation to induce a curvature, and hence refractive change, in a procedure coined "topography-guided CXL."[10] This procedure has the potential to improve the visual outcomes of patients treated for keratoconus or

ectasia,[10] and it could be used as an adjunct therapy in elective refractive surgery procedures for vision correction, or even as a stand-alone minimally invasive alternative in cases requiring low-diopter correction, as demonstrated recently for low myopia, where corrections of 1.00 diopter (D) were achieved at 6 months of follow-up.[11] Further, computational modeling studies have suggested patterned CXL could be effective for addressing astigmatism[12] (eg, postoperative astigmatism associated with cataract surgery and corneal graft surgery). Due to the minimally invasive nature of such a procedure, the popularity of refractive surgery for vision correction, and the high incidence of cataracts in an aging population, the estimated market for this type of treatment is greater than that of conventional refractive surgery, between 8 and 10 million patients per year.[13]

The necessary hardware to conduct customized CXL treatments is already available, because little modification would be required to enable current CXL devices already in widespread use for the treatment of keratoconus to deliver spatially defined treatments. However, to facilitate the widespread adoption of such customized procedures, precise visual outcomes must be achievable, necessitating the development of accurate treatment algorithms. Currently, treatment predictions have been based on either biomechanical models or the outcomes of the limited number of procedures so far undertaken in patients. Biomechanical models have become increasingly advanced in recent years to account for some aspects of the non-linear, anisotropic behavior of the cornea.[14,15] However, to date, much of the biomechanical data underlying these models have been derived either ex vivo from strip extensometry testing or in vivo from air-puff tonometry, via the Ocular Response Analyzer (ORA; Reichert Ophthalmic Instruments) or CorVis Scheimpflug tonometer (CorVis ST; Oculus Optikgeräte GmbH).

The limitations of strip extensometry as a tool for biomechanical evaluation have been well documented.[16] Due to the nature of the measurement procedure and sample preparation, it is now widely acknowledged that strip extensometry does not provide physiologically relevant information capable of relating biomechanics to in vivo behavior and topographic outcomes. With regard to biomechanical assessment via the ORA or CorVis ST, analysis of certain features of the inward and outward movement of the cornea in response to an air-puff has been demonstrated to be valuable for the detection of the presence of biomechanical abnormality.[17-19] However, these methods do not directly measure mechanical properties, with the overall response being a function of stiffness, viscoelasticity, corneal thickness, and an individual's IOP, the relative contribution of each being difficult to distinguish. In addition, the air-puff stimulation used forces the cornea inward, outside its normal range of motion, resulting in flexion of the anterior surface, which normally acts in tension to withstand the normal loads imposed by IOP. Evaluation is also limited to an individual cross-section at a given time. Hence, these methods cannot be used effectively to quantify changes to relevant mechanical properties after treatments and do not provide information with regard to how these treatments and spatial modification of corneal mechanical properties may contribute to changes in refractive outcomes.

A further limitation of existing biomechanical models is that they do not include the limbus and adjacent sclera. This is a consequence of inadequacies of methods to evaluate the biomechanics of these regions.[20] Because recent studies have highlighted the importance of these regions to the biomechanics of the cornea and the maintenance of topography under variations in IOP,[21,22] they cannot be ignored, especially in instances where the goal is to accurately predict refractive outcomes of surgical procedures or CXL.

Assessment of corneal biomechanics is challenging for several reasons, including biological variation, heterogeneity in mechanical properties with respect to location in the tissue, and differential responses to different stimuli, with the magnitude, speed, direction, and position of any stimulus contributing to overall response. Hence, to gain a representative model of corneal biomechanics and understand the association of these properties with topography and pressure compensation, it is necessary to measure the response of the whole cornea under a physiologically representative state of loading. Natural IOP fluctuations, which occur diurnally and during the cardiac cycle, are the primary force to which the cornea is exposed in vivo and the main force responsible, in combination with mechanical properties, integral to controlling its shape. In situ other forces, including forces from the eyelids during blinking and the actions of the extraocular muscles, exert effects and therefore must be considered in a complete model of biomechanics; however, these are significantly harder to simulate and investigate ex vivo. Hence, as a result of IOP being a constant and dominant force on the cornea and the ease with which it can be simulated, most researchers have chosen to examine corneal biomechanics through measuring the deformation of the cornea in response to IOP fluctuations.[23] Several techniques have been investigated, including interferometry-based methods,[2,22,24-28] optical coherence elastography,[29] and high-frequency ultrasound.[30,31]

Recently, displacement speckle pattern interferometry (DSPI) has been used ex vivo for the analysis of corneal biomechanics in response to hydrostatic pressure variations representative of the changes to IOP that occur dur-

ing the normal cardiac cycle.[22] DSPI is a useful tool for the analysis of corneal biomechanics, addressing many of the shortcomings of the more disruptive techniques, such as extensometry. It provides high spatial resolution and high displacement sensitivity, and full surface information can be captured in a single snapshot taking milliseconds, enabling quick and convenient analysis of the cornea and surrounding sclera. Further, because the technique is not destructive and capable of evaluation of the corneal response within its elastic limits, the response of any given cornea can be analyzed before and after procedures such as CXL or refractive surgery, thus enabling each specimen to be used as its own control, avoiding the influence of inter-sample variability in determining the effects of interventions.

A limitation of DSPI is that it measures surface information only and therefore cannot measure any compression that occurs through the thickness of the cornea during loading, preventing full evaluation of corneal strain. However, because the anterior stroma is responsible for the maintenance of corneal curvature and CXL occurs in this region, monitoring changes to surface displacement in response to pressure variations is a logical way to examine the spatial changes to biomechanics that occur due to CXL. Also, optical coherence tomography has previously been used to examine through-thickness changes to the responses of corneas that occur after CXL.[32,33] Hence, information from this study can be used in combination with that provided via other methods to obtain a wholesome view of biomechanical changes.

Recently, a DSPI system and measurement procedure for ex vivo biomechanical analysis of corneoscleral specimens mounted in a modified artificial anterior chamber has been descibed.[22] The efficacy of this approach for examining the biomechanical changes to corneal tissue that can be introduced via CXL in different topographic locations is explored in this study.

MATERIALS AND METHODS
MEASUREMENT AND LOADING SYSTEM
The working principles of DSPI have been described in detail in a previous study.[22] The modified artificial anterior chambers used for mounting corneoscleral specimens and the measurement and loading system that was used for this study are shown diagrammatically in **Figure A** (available in the online version of this article). Illumination was via a diode pumped single-mode solid-state laser (λ = 532 nm) (06-DPL; Cobolt AB), which was expanded and collimated to a diameter of 25 mm. The illumination beam was passed through a 50:50 beamsplitter with half directed toward the target surface (corneal surface) and

half toward a planar mirror attached to a piezoelectric transducer, which was used to generate a phase-stepped reference beam. The beams from the object and the reference were interfered and imaged using a CMOS camera with a resolution of 1,296 by 972 pixels (CMOS Aptina MT9P031; Basler AG) through a 12.5- to 75-mm zoom lens (C31204; Pentax).

The DSPI set-up described is sensitive to out-of-plane (displacement along the z-plane, **Figure AA**) deformation only. To completely define the surface movement, it is necessary to acquire the horizontal (x-plane) and vertical (y-plane) in-plane components of displacement; this is impractical to achieve with interferometry on a curved surface due to the requirement for off-axis imaging and illumination, which gives rise to issues with light intensity variation across the sample. Previous investigations have demonstrated that the in-plane contribution to overall displacement is small relative to the out-of-plane in response to small pressure changes.[22] Hence, in this study focus was on interferometric evaluation of the changes to the out-of-plane response only.

To enable mounting and loading of corneoscleral specimens, artificial anterior chambers were modified by attaching to a reservoir that was mounted onto a motorized vertical translation stage. This enabled convenient, remote, and accurate control of pressure behind the surface of the cornea through modification of the height of the reservoir above the surface of the corneoscleral specimen once situated in the artificial anterior chamber. Movement of the reservoir was controlled using customized software produced using LabView (National Instruments, Inc).

CORNEAL PREPARATION
Four human corneas with an approximately 3-mm scleral boundary were obtained from Moorfield's Biobank (UCL Institute of Ophthalmology), with ethical approval granted by the Moorfields Biobank internal ethics committee. The human corneas were surplus to donor purposes and had been collected with permission for research use. The corneal specimens had been stored for 8 weeks prior to being released for research use. The human corneas were suspended in organ donor culture (80 mL of Eagle's minimum essential medium with HEPES buffer, 26 mmol/l NaHCO3, 2% fetal bovine serum, 2 mmol/L L-glutamine, penicillin, streptomycin, and amphotericin B). All human corneas remained in the solution until required for measurement.

Three fresh porcine eyes (< 12 hours post-mortem) were obtained from a local abattoir (Joseph Morris Butchers). On retrieval, the eyes had clear corneas and intact epitheliums. The corneas with a 2- to 3-mm region of adjacent sclera were isolated from the posterior globe im-

TABLE 1	
CXL Methods	
Parameter	Variable
Treatment target	Refractive
Fluence (total) (J/cm^2)	7.2
Soak time and interval (minutes)	10
Intensity (mW)	15
Treatment time (minutes)	8
Epithelium status	Off
Chromophore	Riboflavin
Chromophore carrier	Saline
Chromophore osmolarity	Isotonic
Chromophore concentration (%)	0.22
Light source	KXL (Avedro, Inc)
Irradiation mode (interval)	Continuous

CXL = corneal cross-linking

mediately prior to testing to enable mounting within the modified artificial anterior chamber (**Figure AA**).

All corneas were deepithelialized prior to measurement. The epithelium has previously been shown to have a negligible contribution to biomechanics,[34] and epithelial debridement was required prior to CXL treatment.

All corneoscleral specimens were mounted within modified artificial anterior chambers (**Figure AA**); these chambers enabled corneas to be hydrostatically loaded while providing a fixed-circular boundary (12.5-mm human corneas, 16-mm porcine corneas) around the scleral rim. On mounting, corneas were subjected to a hydrostatic pressure of 16.5 mm Hg, which is representative of normal IOP in both human and porcine eyes.[35,36] Pressurization was achieved via filling the reservoir and artificial anterior chamber with phosphate-buffered saline solution (Sigma-Aldrich) ($\rho = 0.995$ g/mL at 25°C), then mounting the reservoir 225 mm above the surface of the cornea. All corneas were left to rest at this pressure for 30 minutes prior to the commencement of measurement to allow for stress relaxation. Because the cornea is designed to transmit optical radiation between 400 and 1,400 nm, surface reflection was small at approximately 4%, and had to be enhanced by means of a scattering agent. Hence, prior to interferometric measurement all corneas were coated with a thin layer of hollow glass microspheres (Sphericel 110P8; Potters Industries, LLC), to amplify the scatter from the surface. Due to its particle nature and the fact that it adhered locally to the corneal surface, the surface coating had no stiffness and therefore had no effect on the deformation of the underlying cornea.

EXPERIMENTAL PROCEDURE

Two rounds of interferometric measurement were performed on all corneas: the first round before CXL treatment and the second round after CXL treatment. The measurement procedure consisted of three repeated loading cycles, where the corneas were subjected to pressure increases of 0.25, 0.50, 0.75, and 1.00 mm Hg in turn. At the end of each loading increment, movement of the reservoir was paused for 0.5 second, during which time data were captured and processed, after which the pressure was restored to the baseline pressure.

After the first round of interferometric testing, the surfaces of the corneas were washed using phosphate-buffered saline solution to remove the surface coating. Riboflavin solution (0.22% riboflavin, saline, isotonic) (Vibex-Xtra; Avedro, Inc) was subsequently applied to the entirety of each of the corneal surfaces for a total soaking time of 10 minutes.

Human Cornea CXL Treatment. CXL parameters used are summarized in **Table 1**. For the human corneas, CXL treatment was applied in one of three different topographic regions on an individual cornea. The CXL treatment region selected for each cornea was random and not based on any features observed in the response of the cornea to pressure variations during the initial round of testing. The three different CXL treatment regions that were used across the four specimens are detailed in **Figure 1**. Two of the four corneas had CXL treatment applied in the location shown in **Figure 1A**, with one each of the two remaining corneas undergoing CXL treatment in the locations specified in **Figures 1B-1C**, respectively.

To isolate a specific region for CXL treatment, custom masks were made from aluminum foil to protect the areas of the surface that were not to be subjected to CXL treatment from ultraviolet light exposure. During CXL treatment, the select region on the surface of the cornea was exposed to an ultraviolet-A source at 365 nm (KXL; Avedro, Inc) for 8 minutes at a power of 15 mW/cm^2, delivering a total energy of 7.2 J/cm^2. Total energy delivered during these treatments was maximized because it was desired to introduce a large cross-linking effect during these preliminary experiments to maximize any potential changes to biomechanics. Interferometric measurement after CXL was repeated exactly as specified for testing before CXL.

Porcine Corneas. Porcine Cornea 1 was cross-linked in the location specified in **Figure 1B** and Porcine Cornea 2 was cross-linked in the location specified in **Figure 1C**. The CXL in each case was centered around the corneal apex. Due to the larger size of the porcine corneas, CXL did not extend as close to the periphery as with the human corneas. Hence, for Porcine Cornea 1 a second round of CXL was done to extend
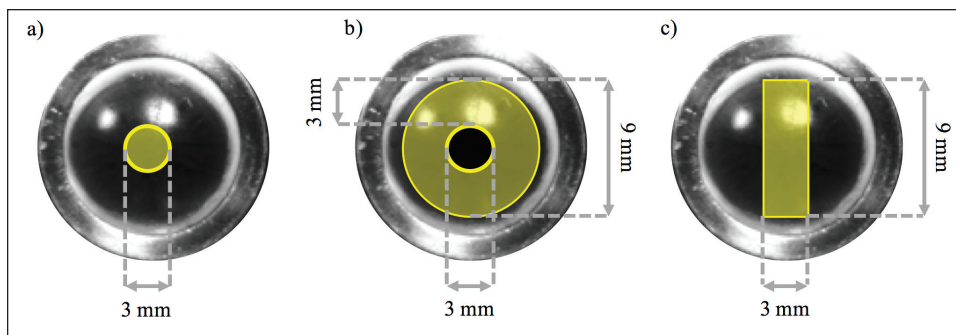
Figure 1. Regions of corneal cross-linking used in human cornea experiments: (A) 3-mm diameter circle at the center of the cornea; (B) 9-mm diameter, 3-mm wide annulus centered on the cornea; and (C) 3-mm width strip positioned down the central 9 mm of the vertical axis.

the CXL region to the scleral region to more closely match the human cornea example.

For Porcine Cornea 3, the region of CXL was determined based on the measured response of the cornea to pressure variations obtained during the first round of interferometric testing. Identification of an abnormal response to loading was determined through knowledge of the expected response of porcine corneas to small pressure variations, which was gained via testing of 40 porcine corneas to small pressure variations, as detailed in a previous study.[22] The particular cornea chosen for this "customized CXL procedure" was selected because there was an unexpectedly large difference in the magnitude of displacement observed over the left and right sides of the nasal-temporal axis during initial testing, with the cornea showing high out-of-plane displacement on the right-side. A custom mask was manufactured from aluminum foil to prevent ultraviolet light exposure over the left side of the cornea. CXL treatment, identical to that described for the human corneas, was conducted on the right side of the nasal-temporal axis only.

DATA ANALYSIS

For the DSPI set-up described, the out-of-plane displacement w (mm) was calculated from the measured phase change due to deformation $\Delta\phi_{def}$(radians) as described by Equation 1, where λ is the wavelength of the illumination source in millimeters.

$$w = \Delta\phi_{def} \cdot \frac{\lambda}{4\pi}$$

The treatment responses of a given cornea to a given pressure variation before and after CXL were compared geographically to determine the effects of CXL on the biomechanical responses.

RESULTS

BEFORE CXL RESPONSE

In general, all human corneas showed similar features in the initial distribution of out-of-plane displacement in response to pressure variations (**Figure 2A**, **Figure 2E**,

Figure 3A, and **Figure 5A**). Across all samples there was a high rate-of-change of out-of-plane displacement at the corneal periphery, indicating high strain in this region, and a relatively constant level of displacement maintained across the central regions, indicating minimal central curvature change of the anterior corneal surface in response to pressure increases. Responses lacked axial symmetry, especially with respect to the nasal-temporal axis. However, some intersample differences in the responses of individual corneas were evident. In particular, the cornea shown in **Figure 5A** had a slightly greater rate of change in out-of-plane displacement across the central regions when compared to the other specimens (**Figure 2A**, **Figure 2E**, and **Figure 3A**).

AFTER CXL RESPONSE

CXL treatment introduced changes to the responses of the corneas to pressure changes. The magnitude and position of these changes was dependent on the area that had undergone CXL treatment. Changes to the responses were not confined to the cross-linked regions in isolation.
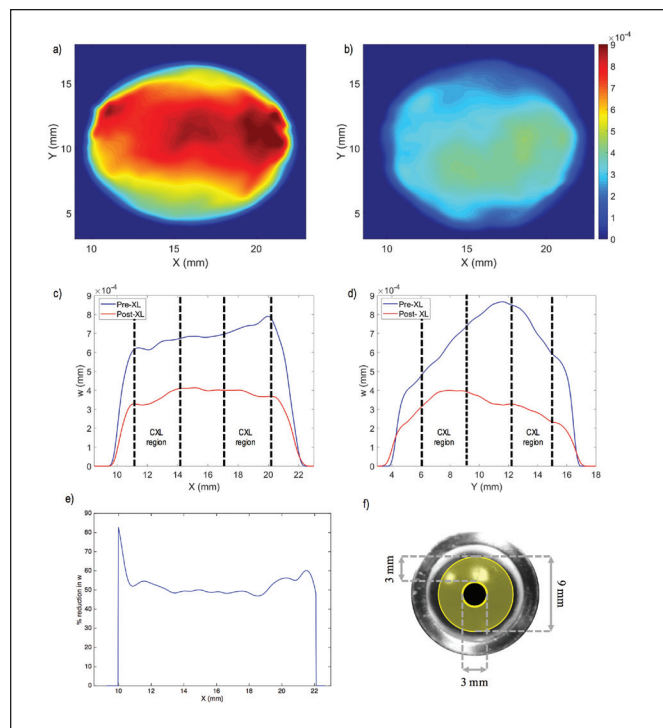
Human Corneas 1 and 2 underwent CXL treatment in a central 3-mm diameter circular region (**Figure 2A**). After CXL treatment, both Human Corneas 1 and 2 showed a reduction in out-of-plane displacement at the center of 16% (**Figure 2**). Both corneas also demonstrated increased displacement relative to the response before CXL in some regions outside of the cross-linked region (**Figure 2C**, **Figure 2G**, and **Figure 2H**), which would indicate a flattening of the corneal topography with respect to these axes when subjected to increases in IOP. Although the reduction in out-of-plane displacement within the cross-linked regions was equivalent for both of the corneas, there were differences with regard to the changes to the responses spatially. This indicates the response to CXL may be variable between corneas and is likely to depend to some extent on initial biomechanics.

Human Cornea 3 underwent CXL treatment in a 9-mm diameter, 3-mm thick annulus centered on the cornea (**Figure 1B**). In comparison to the response before CXL of Human Cornea 3 to an equivalent pressure change, the out-of-plane displacement after CXL was
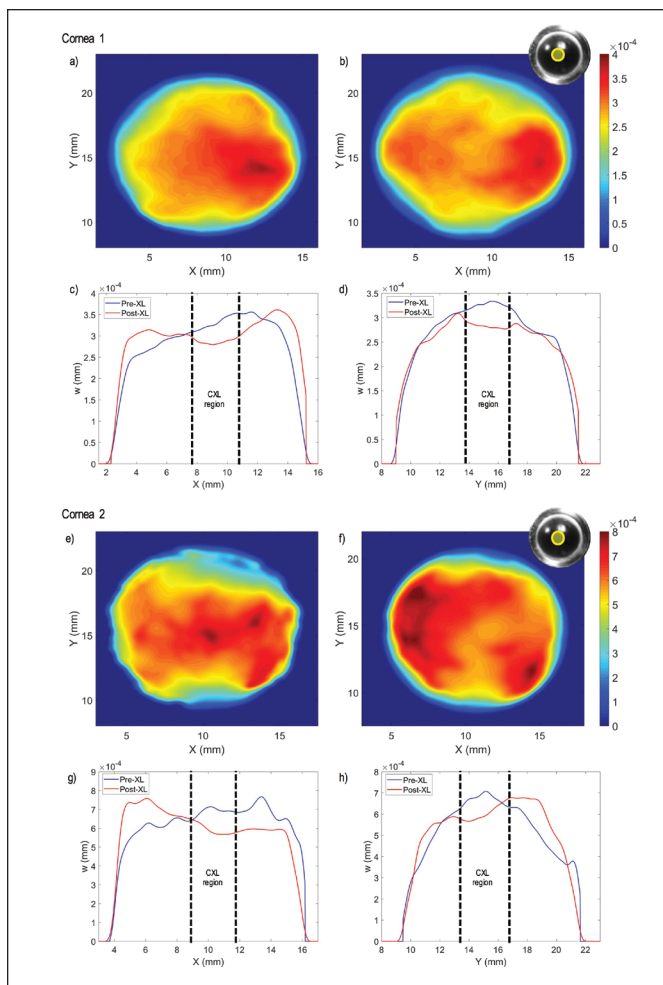
Figure 2. Pre-corneal cross-linking (CXL) vs Post-CXL (central 3 mm) responses of Human Corneas 1 and 2 to pressure variations of 0.25 mm Hg (Cornea 1) and 0.5 mm Hg (Cornea 2) from a baseline pressure of 16.50 mm Hg. For all surface plots blue represents zero displacement and red represents maximum displacement. (A) Pre-CXL displacement of Cornea 1; (B) Post-CXL displacement of Cornea 1; (C) Pre-CXL (blue line) vs Post-CXL (red line) displacement of Cornea 1 along central nasal-temporal axis; (D) Pre-CXL vs Post-CXL displacement of Cornea 1 along central superior-inferior axis; (E) Pre-CXL displacement of Cornea 2; (F) Post-CXL displacement of Cornea 2; (G) Pre-CXL vs Post-CXL displacement of Cornea 2 along central nasal-temporal axis; and (H) Pre-CXL vs Post-CXL displacement of Cornea 2 along central superior-inferior axis.

Figure 3. Pre-corneal cross-linking (CXL) vs Post-CXL (9-mm diameter, 3-mm thick annulus) responses of Human Cornea 3 to pressure variations of 0.5 mm Hg from a baseline pressure of 16.5 mm Hg. (A) Pre-CXL displacement; (B) Post-CXL displacement; (C) Pre-CXL vs Post-CXL displacement along the central nasal-temporal axis; (D) Pre-CXL vs Post-CXL displacement along the central superior-inferior axis; (E) Percentage reduction in out-of-plane displacement Post-CXL along central nasal-temporal axis; and (F) region of CXL.

significantly reduced across the whole surface, including the non-cross-linked region (**Figure 3**). Through spatial analysis of the percentage reduction in out-of-plane displacement in response to a pressure change of 0.5 mm Hg (**Figure 3E**), it was observed that the percentage reduction in displacement was greatest at the periphery, up to 80% in some regions, and lowest in the central non-cross-linked regions at approximately 48%. This would indicate a slight steepening of corneal topography under IOP fluctuations, relative to the case before

treatment. Porcine Cornea 1 had CXL in a similar manner by masking a central 3-mm disk while cross-linking the remaining corneal surface. Similarly to the human cornea, displacement in response to a given pressure change was reduced after CXL (**Figure 4**), although the reduction was less than that seen in the human cornea example. The relative reduction in displacement in the non-cross-linked region was lower, with these regions showing increased deformation relative to immediately adjacent cross-linked regions in response to a pressure increase. Steepening in this zone under increased pressure was evident when looking at the first derivative of displacement, which showed a peak in this region (highlighted as "A" in **Figure 4E**).

Human Cornea 4 and Porcine Cornea 2 underwent treatment along a 3-mm–wide strip down the superior-inferior axis (**Figure 5**). After CXL treatment, Human Cornea 4 showed a significant decrease in out-of-plane displacement in response to a given pressure change, especially along the cross-linked region (**Figure 5D**). In the non-cross-linked regions, there was also a decrease in displacement, but the magnitude of this decrease was
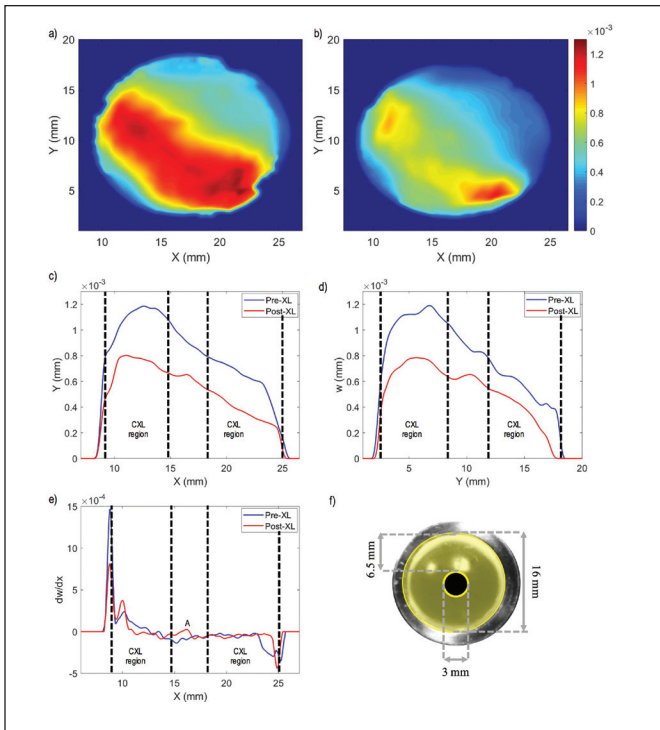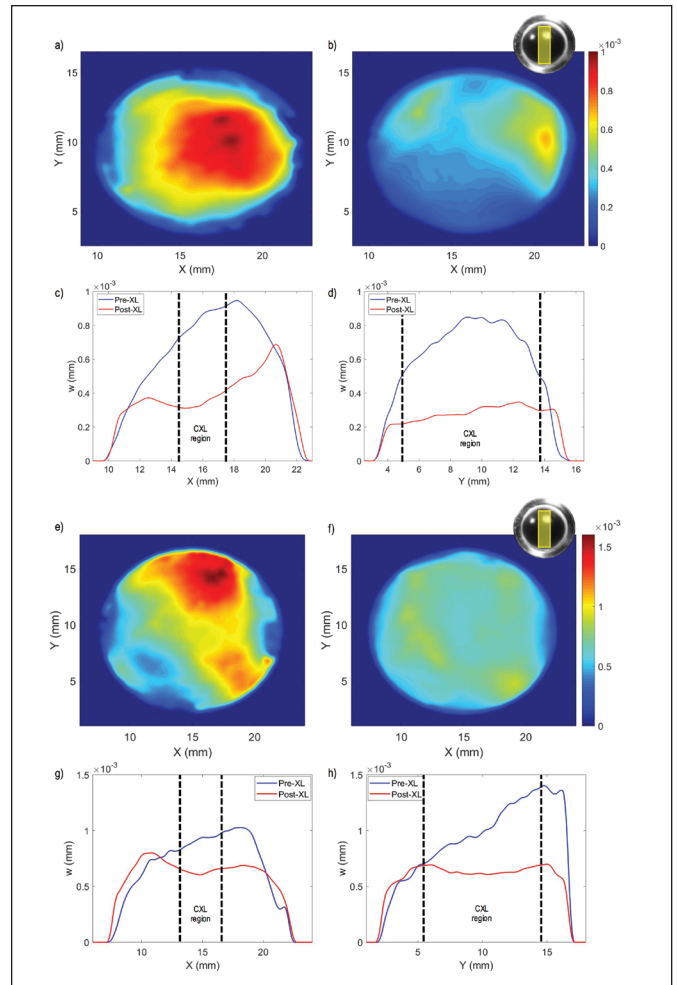
Figure 4. Pre-corneal cross-linking (CXL) vs Post-CXL (annulus around 3-mm diameter masked central region) responses of Porcine Cornea 1 to pressure variations of 0.5 mm Hg from a baseline pressure of 16.5 mm Hg. (A) Pre-CXL displacement; (B) Post-CXL displacement; (C) Pre-CXL vs Post-CXL displacement along the central nasal-temporal axis; (D) Pre-CXL vs Post-CXL displacement along the central superior-inferior axis; (E) first differential of out-of-plane displacement along the nasal-temporal axis, "A" highlights the region of steepening that occurred Post-CXL; and (F) region of CXL.

lower than in the cross-linked regions. The changes to the pattern of displacement introduced would indicate a flattening of corneal topography with respect to the nasal-temporal axis (normal to the axis of CXL treatment) due to relatively higher deformation at the periphery relative to the center along this axis. The changes to the response of Porcine Cornea 2 were similar to those observed in the human cornea, with a reduction in displacement along the cross-linked region especially (**Figures 5G-5H**) and a flattening of corneal topography in response to increased pressure along the nasal-temporal axis perpendicular to the cross-linked axis (**Figure 5G**). However, the relative reduction in displacement due to CXL in the porcine cornea was less than in the human cornea.

CUSTOMIZED CXL

The treatment response before CXL of the porcine cornea to small pressure variations showed abnormally high out-of-plane displacement on the right side of the nasal-temporal axis relative to the left side (**Figure 6A**). Treatment was isolated to the right side of

Figure 5. Pre-corneal cross-linking (CXL) and Post-CXL (central 3-mm wide strip down superior-inferior axis) responses of Human Cornea 4 and Porcine Cornea 2 to pressure variations of 0.5 mm Hg from a baseline pressure of 16.5 mm Hg. (A) Pre-CXL displacement of Human Cornea 4; (B) Post-CXL displacement of Human Cornea 4; (C) Pre-CXL vs Post-CXL displacement along central nasal-temporal axis of Human Cornea 4; (D) Pre-CXL vs Post-CXL displacement along central superior-inferior axis of Human Cornea 4; (E) Pre-CXL displacement of Porcine Cornea 2; (F) Post-CXL displacement of Porcine Cornea 2; (G) Pre-CXL vs Post-CXL displacement along central nasal-temporal axis of Porcine Cornea 2; and (H) Pre-CXL vs Post-CXL displacement along central superior-inferior axis of Porcine Cornea 2.

the cornea (**Figure 6D**. After CXL, the displacement response of the right side of the cornea was significantly reduced compared to the response before treatment (**Figures 6B-6C**). The magnitude of out-of-plane displacement across the corneal surface became more uniform overall, with displacement on the left and right sides of the cornea, becoming approximately equal. Two regions of slightly higher displacement toward the top and bottom of the cornea remained (**Figure 6B**) and these corresponded to the areas outside the 9-mm diameter ultraviolet light beam, and there-
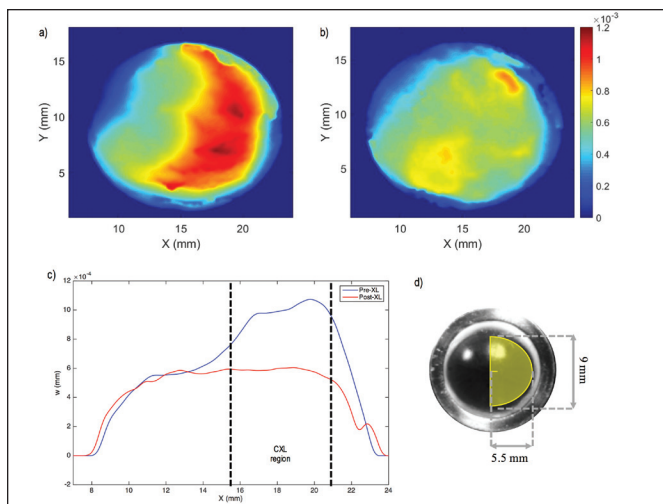
Figure 6. Pre-corneal cross-linking (CXL) vs Post-CXL (right-side only) responses of a porcine cornea to a 0.5 mm Hg increase in pressure from a baseline pressure of 16.5 mm Hg. (A) Pre-CXL displacement; (B) Post-CXL displacement; (C) Pre-CXL vs Post-CXL displacement along the central nasal-temporal axis; (D) Region of cross-linking.

fore had no direct exposure and were assumed to have undergone minimal CXL.

DISCUSSION

The application of CXL treatment across different topographic regions had location-specific effects. The rationale for stiffening the cornea in isolated regions is to introduce spatially specific changes to the mechanical properties of the tissue, which in turn would be expected to lead to modifications in topography and refractive power. Ultimately, the aim is to facilitate the delivery of customized CXL treatment, with treatment parameters and locations determined based on the biomechanics and topography of an individual cornea. However, achieving accurate and optimized visual outcomes via this approach requires a method to spatially quantify corneal biomechanics in vivo, an understanding of the normal biomechanics of the cornea and their contribution to topography, and detailed knowledge of the effects of CXL treatment on corneal biomechanics and associated long-term topographic changes.

Currently there is no established method to spatially quantify corneal mechanical properties in vivo. Several methods are currently being investigated to achieve this, including Brillouin spectroscopy,[37] optical coherence elastography,[29] and high-frequency ultrasound.[31] All of these techniques require scanning to generate whole-corneal information, requiring acquisition times of several minutes, leading to limited spatial resolutions and issues with motion artifacts when attempting to quantify whole-corneal mechanical properties in clinic. Hence, none so far have reached the stage of widespread clini-

cal adoption. Because biomechanics and topography are inherently related, in the clinic we currently rely on detailed topographic assessment to provide an indication of the presence of abnormalities in biomechanics. The disadvantage of this is that we require progression to a stage where abnormalities in topography are present prior to diagnosis. This could be avoided with the introduction of a sensitive test to probe mechanical properties, allowing abnormalities to be identified and treated at onset, prior to any symptomatic changes in topography.

The introduction of a clinical device capable of biomechanical evaluation is important, but the method detailed in this study aimed to address the latter two requirements: an understanding of normal corneal biomechanics and their contribution to topography and the effects of CXL. This is achieved through spatial quantification of normal biomechanics under physiological loading and detailed assessment of the effects of location-specific CXL treatment on this response. Although a relatively small sample size was used in this study, the purpose, at this stage, was to demonstrate the ability of the technique described to spatially map changes associated with biomechanics after CXL treatment. The technique has demonstrated efficacy in its ability to both recognize abnormal patterns in the initial response of corneas to pressure variations and spatially map changes related to the biomechanics of corneas after application of CXL treatment. This is the first study to investigate these effects on human corneas.

Analyzing the deformation and biomechanics of the anterior corneal surface is particularly important when considering topography, because Bowman's layer and anterior stroma are the regions most important to maintaining corneal shape and refractive power. Sensing biomechanical changes to the response of the anterior surface to pressure variations provides insight into likely topographic changes that will occur over time as the system comes to a steady state after treatment.

Overall the nature of the response of the human corneas before CXL used in this study were consistent with several previous studies that have indicated high axial compliance at the limbus.[21,22,38,39] Application of CXL treatment in the three areas described in **Figure 1** resulted in different effects and these effects showed a logical correlation with treatment area, indicating that the changes observed were a result of ultraviolet light exposure.

CXL treatment in the central region only would be assumed to induce corneal flattening, and potentially myopic correction through increased resistance of the central cornea to deformation under IOP, leading to a compensatory increase in deformation in surrounding regions to accommodate for the pressure increase. This effect was observed in both human corneas that were stiffened in

this region. Not only was there an increase in the resistance of the central region to deformation (16% reduction in out-of-plane displacement in response to hydrostatic pressure increase from 16.5 to 17 mm Hg), but there was a compensatory increase in deformation in the regions outside of this, further enhancing the flattening effect.

There were clear similarities between the two corneas examined in terms of the changes to the responses bought about by CXL in this region, especially with regard to the reduction in displacement within the cross-linked region. However, there were also subtle differences, possibly related to baseline biomechanics. Due to this variation in the treatment response, it is evident that to develop accurate treatment algorithms, it will be necessary to examine a large number of corneas.

CXL at the periphery while masking the central region would be expected to increase the resistance of the outer regions of the cornea to deformation under variations in IOP, with a compensatory relative increase in displacement in the center relative to the adjacent cross-linked regions. This type of treatment would be proposed for conditions where steepening the curvature of the cornea would be advantageous, such as hyperopia. For both the human and porcine corneas treated in this way, there was a large reduction in out-of-plane displacement in response to a given pressure change across the full surface. The reduction was greater in the human cornea versus the porcine cornea, which is likely due to the greater thickness of the porcine cornea relative to the human cornea, resulting in a lesser percentage of the total stromal depth undergoing CXL. This type of treatment was expected to provide a larger reduction in displacement when compared with CXL of the central region only, because a larger area of the cornea underwent CXL, and the CXL was focused on the region that had previously shown the highest rate of displacement in response to pressure variations.

On close examination, the reduction in displacement in the central non–cross-linked regions was lower than in the regions that had been cross-linked (48% vs 50% to 80% reduction in the human cornea) (**Figure 3E**), indicative of a slight steepening effect, which was in line with initial predictions. However, our results and previous results demonstrating the relative lower axial strength of the peripheral cornea and the limbus relative to the central regions suggest that it would be challenging to achieve a large steepening effect. This is because the relatively low axial stiffness of the limbus and peripheral cornea versus the central cornea means that the aforementioned regions overwhelmingly compensate for small pressure variations with little curvature change across the central regions.[22] Even after CXL in the outer regions, most of the strain remained concentrated within these regions, with displacement

across the central cornea remaining relatively uniform, indicating high resistance to changes in central curvature. It could be that certain modifications to the treatment applied here, such as reducing the thickness of the annulus or CXL at a different proximity to the limbus, could produce a more significant steepening effect. However, these remain to be explored in future studies.

The reason for CXL along a specific axis in isolation (**Figure 1C**) would be to change the relative stiffness of one axis compared to the other, to modify the axial curvature, and to address astigmatism. For the cornea examined, CXL in a strip along the superior-inferior axis did significantly reduce displacement in response to a given pressure change along this axis by up to 75% in the human cornea and introduced axial-specific modifications to curvature, resulting in a flattening effect across the nasal-temporal axis in response to increases in chamber pressure. Again, the changes to the distribution of displacement that occurred before versus after CXL were similar in the human and porcine corneas, but the porcine cornea showed a lower overall reduction, likely due to the reasons already discussed.

Finally, a demonstration of customized CXL was attempted, although the visual outcomes of this treatment could not be quantified in this study. The potential for interferometry to identify a region of relative biomechanical weakness was demonstrated here, and a customized mask was designed for CXL treatment. The CXL treatment appeared to normalize the responses of the left and right sides of the cornea. This final experiment provides an initial demonstration of the potential application of CXL technology if it can be combined with clinical full-field assessment of biomechanics and detailed knowledge of normal corneal biomechanics and the effects of CXL.

The advantages of customized CXL if it can be accurately delivered are many. There is already evidence that targeted treatment may have advantages over conventional treatment in the management of keratoconus[10] in addition to evidence that customized treatments may have the potential to be used as an alternative to invasive refractive surgery for cases of low-diopter correction[11] and mild astigmatism.[12] They also could be employed as an adjunct therapy in other cases, reducing the amount of tissue that would need to be removed and enhancing the strength of the cornea postoperatively, reducing the incidence of complications and increasing the long-term stability of outcomes. Similar advantages could also be achieved via the use of CXL as an adjunct therapy in corneal transplant and cataract surgeries.

The ability of CXL to deliver location-specific alterations to biomechanics has been demonstrated in this study. However, the changes that occur are complex

hence to produce treatment algorithms capable of delivering alterations in biomechanics that translate to precise and accurate changes in refractive power requires both testing on a large number of corneas and the use of several complementary techniques in addition to the interferometric method described here to provide a full assessment and understanding of the changes that occur after CXL treatment. To truly understand the potential of the CXL technique for delivering customized and optimized treatments, its ability to produce repeatable biomechanical changes must be investigated. As demonstrated in this study, there is significant variability between the biomechanics of individual corneas prior to CXL treatment and it is likely that the response of corneas to CXL will also be variable to some degree, due to factors such as age, genetics, and environment. Hence, a study with a sufficiently large sample size, where the aforementioned factors can be accounted for, is required to begin the development of the necessary treatment models that would be required for optimized delivery of CXL.

DSPI has been shown to be an effective tool for the assessment of the changes that occur to corneal anterior surface displacement in response to physiological scale pressure variations before and immediately after CXL. It is likely the changes to the distribution of displacement of the anterior corneal surface that are observed after CXL will provide a useful indicator of the topographic changes that will occur over the recovery time.

The design of the study, which enables the same cornea to be examined before and after CXL treatment under physiological scale pressure variations, is particularly advantageous because it enables inter-sample variability to be accounted for and ensures the measurements remain relevant to the in vivo case. The measurement procedure is highly efficient, taking only milliseconds to generate full-surface information. The information provided by DSPI represents the anterior manifestation of the bulk changes in properties of a three-dimensional tissue, providing useful insight into the likely long-term topographic effects of such treatments, but in isolation is not enough to quantify stiffness changes in the absence of through-thickness information. Going forward, it would be useful to use this information together with that from methods such as optical coherence tomography[33] or high-frequency ultrasound,[31] which are capable of examining the through-thickness responses of corneas to pressure variations, allowing us to generate three-dimensional data on biomechanical changes. A combination of these approaches provides an optimal solution because the fast, whole-surface measurement advantages of DSPI could be used to direct targeted through-thickness measurements with optical coherence tomography or high-frequency ultrasound, which due to their requirement for scanning to acquire three-dimensional information have relatively long acquisition times when used alone.

Ultimately, to deliver precise refractive outcomes, it is necessary to understand the relationship between biomechanical and longer-term topographic changes and refractive outcomes. This can be particularly challenging to investigate because topographic changes have been documented to continue for several months to years after CXL treatment in patients with keratoconus.[6,40] It is possible that through combining the information gained on the biomechanical effects of CXL through studies such as this one with clinical studies that document the longer-term topographic effects of CXL, it will be possible to accurately model and predict long-term topographic outcomes, moving us closer to customization and optimization of CXL treatments.

The DSPI method described has the potential to contribute to the optimization of the delivery of CXL treatment through enabling effects of many of the variables associated with the effectiveness of the treatment, such as treatment time, location, power, and oxygen concentration to be investigated.

AUTHOR CONTRIBUTIONS

Study concept and design (AW, JM); data collection (AW, JJ); analysis and interpretation of data (AW, JJ); writing the manuscript (AW); critical revision of the manuscript (JJ, JM); statistical expertise (AW, JM); administrative, technical, or material support (JM); supervision (JM)

REFERENCES

1. Wollensak G, Iomdina E. Long-term biomechanical properties of rabbit cornea after photodynamic collagen crosslinking. *Acta Ophthalmol.* 2009;87(1):48-51. doi:10.1111/j.1755-3768.2008.01190.x

2. Knox Cartwright NE, Tyrer JR, Marshall J. In vitro quantification of the stiffening effect of corneal cross-linking in the human cornea using radial shearing speckle pattern interferometry. *J Refract Surg.* 2012;28(7):503-508. doi:10.3928/1081597X-20120613-01

3. Meek KM, Hayes S. Corneal cross-linking—a review. *Ophthalmic Physiol Opt.* 2013;33(2):78-93. doi:10.1111/opo.12032

4. Wollensak G, Spoerl E, Seiler T. Riboflavin/ultraviolet-a-induced collagen crosslinking for the treatment of keratoconus. *Am J Ophthalmol.* 2003;135(5):620-627. doi:10.1016/S0002-9394(02)02220-1

5. Vinciguerra P, Albè E, Trazza S, Seiler T, Epstein D. Intraoperative and postoperative effects of corneal collagen cross-linking on progressive keratoconus. *Arch Ophthalmol.* 2009;127(10):1258-1265. doi:10.1001/archophthalmol.2009.205

6. O'Brart DP, Kwong TQ, Patel P, McDonald RJ, O'Brart NA. Long-term follow-up of riboflavin/ultraviolet A (370 nm) corneal collagen cross-linking to halt the progression of keratoconus. *Br J Ophthalmol.* 2013;97(4):433-7. doi:10.1136/bjophthalmol-2012-302556

7. Raiskup F, Theuring A, Pillunat LE, Spoerl E. Corneal collagen crosslinking with riboflavin and ultraviolet-A light in progressive keratoconus: ten-year results. *J Cataract Refract Surg.* 2015;41(1):41-46. doi:10.1016/j.jcrs.2014.09.033

8. Mazzotta C, Moramarco A, Traversi C, Baiocchi S, Iovieno A, Fontana L. Accelerated corneal collagen cross-linking using topography-guided UV-A energy emission: preliminary clinical and morphological outcomes. *J Ophthalmol.* 2016;2016:2031031. doi:10.1155/2016/2031031

9. Nordström M, Schiller M, Fredriksson A, Behndig A. Refractive improvements and safety with topography-guided corneal crosslinking for keratoconus: 1-year results. *Br J Ophthalmol.* 2017;101(7):920-925. doi:10.1136/bjophthalmol-2016-309210

10. Cassagne M, Pierné K, Galiacy SD, Asfaux-Marfaing MP, Fournié P, Malecaze F. Customized topography-guided corneal collagen cross-linking for keratoconus. *J Refract Surg.* 2017;33(5):290-297. doi:10.3928/1081597X-20170201-02

11. Elling M, Kersten-Gomez I, Dick HB. Photorefractive intrastromal corneal crosslinking for the treatment of myopic refractive errors: six-month interim findings. *J Cataract Refract Surg.* 2017;43(6):789-795. doi:10.1016/j.jcrs.2017.03.036

12. Seven I, Sinha Roy A, Dupps WJ Jr. Patterned corneal collagen crosslinking for astigmatism: computational modeling study. *J Cataract Refract Surg.* 2014;40(6):943-953. doi:10.1016/j.jcrs.2014.03.019

13. Nataloni R. Q&A with David Muller, PhD, MBA. *Cataract Refract Surgery Today.* Published June 2015. https://crstoday.com/articles/2015-jun/qa-with-david-muller-phd-mba/

14. Nejad TM, Foster C, Gongal D. Finite element modelling of cornea mechanics: a review. *Arq Bras Oftalmol.* 2014;77(1):60-65.

15. Seven I, Dupps WJ. Patient-specific finite element simulations of standard incisional astigmatism surgery and a novel patterned collagen crosslinking approach to astigmatism treatment. *J Med Device.* 2013;7(4):0409131-409132. doi:10.1115/1.4025980

16. Elsheikh A, Anderson K. Comparative study of corneal strip extensometry and inflation tests. *J R Soc Interface.* 2005;2(3):177-185. doi:10.1098/rsif.2005.0034

17. Ventura BV, Machado AP, Ambrósio R Jr, et al. Analysis of waveform-derived ORA parameters in early forms of keratoconus and normal corneas. *J Refract Surg.* 2013;29(9):637-643. doi:10.3928/1081597X-20130819-05

18. Vinciguerra R, Ambrósio R Jr, Elsheikh A, et al. Detection of keratoconus with a new biomechanical index. *J Refract Surg.* 2016;32(12):803-810. doi:10.3928/1081597X-20160629-01

19. Vinciguerra R, Ambrósio R Jr, Roberts CJ, Azzolini C, Vinciguerra P. Biomechanical characterization of subclinical keratoconus without topographic or tomographic abnormalitites. *J Refract Surg.* 2017;33(6):399-407. doi:10.3928/1081597X-20170213-01

20. Pandolfi A. Cornea modelling. *Eye Vis (Lond).* 2020;7:2. doi:10.1186/s40662-019-0166-x

21. Boyce BL, Grazier JM, Jones RE, Nguyen TD. Full-field deformation of bovine cornea under constrained inflation conditions. *Biomaterials.* 2008;29(28):3896-3904. doi:10.1016/j.biomaterials.2008.06.011

22. Wilson A, Jones J, Tyrer JR, Marshall J. An interferometric ex vivo study of corneal biomechanics under physiologically representative loading, highlighting the role of the limbus in pressure compensation. *Eye Vis (Lond).* 2020;7(1):43. doi:10.1186/s40662-020-00207-1

23. Wilson A, Marshall J. A review of corneal biomechanics: mechanisms for measurement and the implications for refractive surgery. *Indian J Ophthalmol.* 2020;68(12):2679-2690. doi:10.4103/ijo.IJO_2146_20

24. Jaycock PD, Lobo L, Ibrahim J, Tyrer J, Marshall J. Interferometric technique to measure biomechanical changes in the cornea induced by refractive surgery. *J Cataract Refract Surg.* 2005;31(1):175-184. doi:10.1016/j.jcrs.2004.10.038

25. Knox Cartwright NE, Tyrer JR, Marshall J. Age-related differences in the elasticity of the human cornea. *Invest Ophthalmol Vis Sci.* 2011;52(7):4324-4329. doi:10.1167/iovs.09-4798

26. Knox Cartwright NE, Tyrer JR, Jaycock PD, Marshall J. Effects of variation in depth and side cut angulations in LASIK and thin-flap LASIK using a femtosecond laser: a biomechanical study. *J Refract Surg.* 2012;28(6):419-425. doi:10.3928/1081597X-20120518-07

27. Wilson A, Marshall J, Tyrer JR. The role of light in measuring ocular biomechanics. *Eye (Lond).* 2016;30(2):234-240. doi:10.1038/eye.2015.263

28. Wilson A, Marshall J. A speckle interferometric technique for the evaluation of corneal biomechanics under physiological pressure variations (Conference Presentation). Proc. SPIE 10880, Optical Elastography and Tissue Biomechanics VI, 108800Z (March 13, 2019). doi:10.1117/12.2507660

29. Nair A, Singh M, Aglyamov SR, Larin KV. Heartbeat OCE: corneal biomechanical response to simulated heartbeat pulsation. *J Biomed Opt.* 2020;25(5):055001. doi:10.1117/1.JBO.25.5.055001

30. Pavlatos E, Chen H, Clayson K, Pan X, Liu J. Imaging corneal biomechanical responses to ocular pulse using high-frequency ultrasound. *IEEE Trans Med Imaging.* 2018;37(2):663-670. doi:10.1109/TMI.2017.2775146

31. Clayson K, Pavlatos E, Pan X, Sandwisch T, Ma Y, Liu J. Ocular pulse elastography: imaging corneal biomechanical responses to simulated ocular pulse using ultrasound. *Transl Vis Sci Technol.* 2020;9(1):5. doi:10.1167/tvst.9.1.5

32. Palko JR, Tang J, Cruz Perez B, Pan X, Liu J. Spatially heterogeneous corneal mechanical responses before and after riboflavin-ultraviolet-A crosslinking. *J Cataract Refract Surg.* 2014;40(6):1021-1031. doi:10.1016/j.jcrs.2013.09.022

33. Kling S. Optical coherence elastography by ambient pressure modulation for high-resolution strain mapping applied to patterned cross-linking. *J R Soc Interface.* 2020;17(162):20190786. doi:10.1098/rsif.2019.0786

34. Elsheikh A, Alhasso D, Rama P. Assessment of the epithelium's contribution to corneal biomechanics. *Exp Eye Res.* 2008;86(2):445-451. doi:10.1016/j.exer.2007.12.002

35. Ruiz-Ederra J, García M, Hernández M, et al. The pig eye as a novel model of glaucoma. *Exp Eye Res.* 2005;81(5):561-569. doi:10.1016/j.exer.2005.03.014

36. Schneider E, Grehn F. Intraocular pressure measurement-comparison of dynamic contour tonometry and goldmann applanation tonometry. *J Glaucoma.* 2006;15(1):2-6. doi:10.1097/01.ijg.0000196655.85460.d6

37. Seiler TG, Shao P, Eltony A, Seiler T, Yun SH. Brillouin spectroscopy of normal and keratoconus corneas. *Am J Ophthalmol.* 2019;202:118-125. doi:10.1016/j.ajo.2019.02.010

38. Hjortdal JOØ. Regional elastic performance of the human cornea. *J Biomech.* 1996;29(7):931-942. doi:10.1016/0021-9290(95)00152-2

39. Whitford C, Joda A, Jones S, Bao F, Rama P, Elsheikh A. Ex vivo testing of intact eye globes under inflation conditions to determine regional variation of mechanical stiffness. *Eye Vis (Lond).* 2016;3(1):21. doi:10.1186/s40662-016-0052-8

40. Nicula C, Pop R, Rednik A, Nicula D. 10-year results of standard cross-linking in patients with progressive keratoconus in Romania. *J Ophthalmol.* 2019;2019:8285649. doi:10.1155/2019/8285649
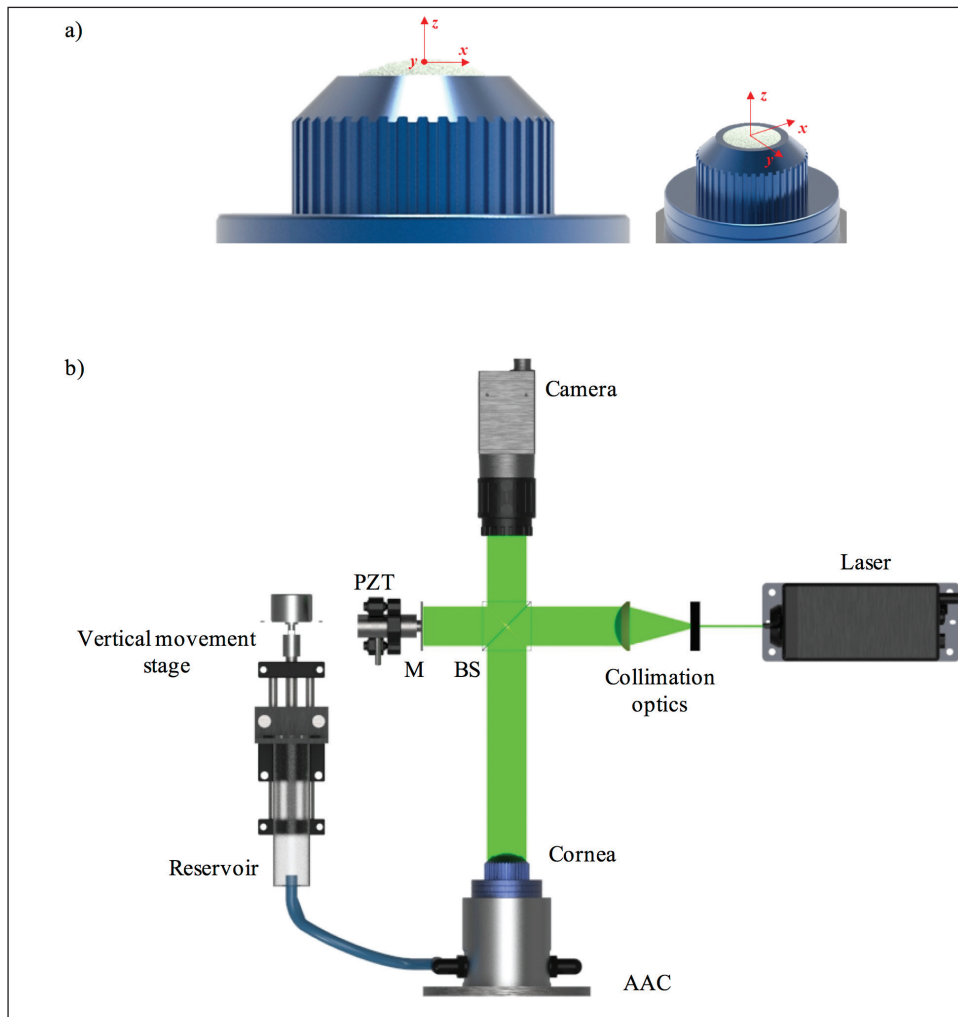
Figure A. Measurement set-up showing (A) artificial anterior chamber and (B) displacement speckle pattern interferometry (DSPI) configuration and corneal mounting and pressurization apparatus. AAC = artificial anterior chamber; BS = beamsplitter; M = mirror; PZT = piezoelectric transducer